# Attitude determination designs for the GOES spacecraft

John L. Crassidis, F. Landis Markley, Arthur M. Kyle

Goddard Space Flight Center
Guidance and Control Branch, Code 712
Greenbelt, MD 20771

Kathie Blackman

Orbital Sciences Corporation
7500 Greenway Center Drive, Suite 700
Greenbelt, MD 20770

## ABSTRACT

This paper presents a summary of the basic simulation parameters and results of a study for the Geostationary Operational Environmental Satellite (GOES). The study involves the simulation of minor modifications to the current spacecraft, so that the relative performance of these modifications can be analyzed. The first modification studied requires the placement of a baseline inertial reference unit, such as the Dry Rotor Inertia Reference Unit (DRIRU-II) or the Space Inertial Reference Unit (SIRU), onto the spacecraft. The second modification involves using the imager/sounder assembly for real-time on-board attitude determination information. The third modification studied is the addition of star trackers to provide precise attitude knowledge. Simulation results are presented for each modification.

KEYWORDS: Earth Sensor, Star Tracker, QUEST, Enhanced QUEST, Kalman Filter

## 1. INTRODUCTION

In this paper, a design study is shown for attitude determination of the Geostationary Operational Environmental Satellite (GOES). The current (GOES-8) spacecraft specification for the knowledge requirement is 112 μrad. This requirement is met through ground processing 99% of the time in the east/west direction and 95% of the time in the north/south direction. The spacecraft specification for the within-frame image registration is 42 μrad. This requirement is met through ground processing 90% of the time in the east/west direction and 70% of the time in the north/south direction. The current spacecraft uses an Earth Sensor Assembly (ESA) to provide roll and pitch information. A set of gyros, the Digital Integration Rate Assembly (DIRA), also is on the current spacecraft. However, the DIRA has an operational lifetime of 2000 hours. Therefore, the on-board gyros are not used for mission mode attitude determination and control.

A number of new attitude determination schemes and hardware modifications is presented. The first modification involves the addition of high precision gyros, such as the Dry Rotor Inertia Reference Unit (DRIRU-II) or Space Inertial Reference Unit (SIRU), onto the spacecraft with the existing ESA. Simulation results are presented using a Kalman filter for attitude determination.

The imager/sounder assembly is currently used to obtain landmark and/or star observations in order to compensate for spacecraft motions and external disturbances through ground processing. The second modification utilizes the imager/sounder assembly as another attitude sensor for on-board attitude determination. This provides a means to supplement the ESA determined attitude, as well as providing yaw information. Simulation results are also presented using a Kalman filter for attitude determination.

The final modification involves the addition of star trackers with or without high precision gyros to provide precise attitude knowledge. The proposed GOES attitude determination system includes one or two star trackers. A covariance analysis is first shown to determine the optimal orientations of the star trackers. Next, an actual star availability analysis is shown using the optimal tracker orientations and GOES orbit. The QUEST[1] algorithm is used for attitude determination without gyros. In order to further improve attitude knowledge an enhanced QUEST algorithm is also utilized. This involves a simple first-order Kalman filter type algorithm to filter noisy star measurements. Finally, simulation results for all case studies are presented.

## 2. EARTH SENSOR, IMAGER/SOUNDER

In this section, a brief overview of the simulation parameters for the gyro model, the ESA model, and the imager/sounder model is shown. The true angular velocity is assumed to be modeled by[2]

$$\underline{\omega} = \underline{\widetilde{\omega}}_g - \underline{b} - \underline{\eta}_1 \tag{1}$$

where $\underline{\omega}$ is the true angular velocity, $\underline{\widetilde{\omega}}_g$ is the gyro-determined angular velocity, and $\underline{b}$ is the gyro drift vector,

$$\dot{\underline{b}} = \underline{\eta}_2 \tag{2}$$

The $3\times 1$ vectors, $\underline{\eta}_1$ and $\underline{\eta}_2$, are assumed to be modeled by a Gaussian white-noise process with

$$E\left\{\underline{\eta}_i(t)\right\} = \underline{0} \qquad i = 1, 2 \tag{3}$$

$$E\left\{\underline{\eta}_i(t)\underline{\eta}_j^T(t')\right\} = Q_i\,\delta_{ij}\,\delta(t-t') \qquad i, j = 1, 2 \tag{4}$$

where

$$Q_1 = \sigma_v^2 I_{3\times 3} \tag{5a}$$

$$Q_2 = \sigma_u^2 I_{3\times 3} \tag{5b}$$

The DRIRU-II drift-rate noise and measurement noise characteristics are given by $\sigma_u = 2.15\times 10^{-4}\ \mu\text{rad}/\text{sec}^{3/2}$ and $\sigma_v = 0.206\ \mu\text{rad}/\text{sec}^{1/2}$. The nominal motion of the spacecraft involves a rotation once per orbit about the spacecraft's y-axis. Therefore, the nominal angular velocity is given by

$$\underline{\omega} = \begin{bmatrix} 0 \\ \omega_n \\ 0 \end{bmatrix} \tag{6}$$

where $\omega_n$ is the orbit rotation rate $\left(7.27\times 10^{-5}\ \text{rad}/\text{sec}\right)$.

The ESA measures the spacecraft's roll and pitch angles. These angles are measured with respect to a moving Earth frame. The gyros provide attitudes with respect to an inertially fixed frame (e.g., GCI). Since the body rotation axis is about the spacecraft's y-axis, the body measurement vector is given by[3]

$$\underline{B}_e = \begin{bmatrix} -\sin(p)\cos(r) \\ \sin(r) \\ \cos(p)\cos(r) \end{bmatrix} \tag{7}$$

where $r$ and $p$ are the scanner roll and pitch angles, respectively. The inertial reference vector is given by

$$\underline{I}_e = A^T(q)\,\underline{B}_e \tag{8}$$

where $q$ is the true quaternion (obtained by kinematic propagation using the true angular velocity). The ESA "measurements" are obtained by using the following model

$$\widetilde{p} = p + v_p + w_p \tag{9}$$

where $v_p$ is a zero-mean Gaussian process with a $3\sigma$ value of 0.02 degrees, and $w_p$ represents the non-repeatable errors due to Earth cloud and Earth radiance/gradients effects. The non-repeatable error is assumed to be modeled by the following discrete process

$$w_p(i+1) = A\, w_p(i) + L\left(1 - A^2\right)^{1/2} g(i) \tag{10a}$$

$$A = \exp(-4\,\Delta t\, B) \tag{10b}$$

where $\Delta t$ is the sampling interval (0.25 seconds for the ESA), $B$ is the bandwidth (for weather purposes, this set to about 1/6 days), $L$ is the $1\sigma$ amplitude (experience has shown that this is about 200 $\mu$rad ), and $g$ is a zero-mean normal Gaussian process. This same error model is applied to the Earth roll "measurement." Since the roll and pitch measurements from the Earth sensor are small, the body measurements can be approximated by

$$\underline{\tilde{B}}_B^e \approx \begin{bmatrix} -\tilde{p} \\ \tilde{r} \\ 1 \end{bmatrix} \tag{11}$$

The imager/sounder assembly can measure stars in a $23^\circ\,\mathrm{E/W} \times 21^\circ\,\mathrm{N/S}$ field of view, outside of the Earth limb. The orbit-attitude tracking system contains a catalog of bright stars visible by the imager/sounder which typically senses three stars at 45 second intervals. For simulation purposes these stars are assumed to be found in different quadrants in the field of view. Each instrument performs a star look every 30 minutes. The imager/sounder measures the tangent of two angles, $\beta_1$ and $\beta_2$ , resulting in a body vector given by[3]

$$\underline{B}_{i/s} = \frac{1}{\sqrt{1 + \tan^2\beta_1 + \tan^2\beta_2}} \begin{bmatrix} \tan\beta_1 \\ \tan\beta_2 \\ 1 \end{bmatrix} \tag{12}$$

The imager/sounder "measurements" are obtained by using the following model

$$\tan\tilde{\beta}_i = \tan\beta_i + v_{bi} + w_{bi}, \qquad i = 1, 2 \tag{13}$$

where $v_b$ is a zero-mean Gaussian process with a $3\sigma$ value of 28 $\mu$rad . The non-repeatable error in the imager/sounder is assumed to be modeled by the following process

$$\dot{\underline{x}} = \begin{bmatrix} 0 & 1 \\ -\omega_n^2 & 0 \end{bmatrix} \underline{x} + \begin{bmatrix} 0 \\ 1 \end{bmatrix} \eta \tag{14a}$$

$$w_b = \begin{bmatrix} 1 & 0 \end{bmatrix} \underline{x} \tag{14b}$$

where $\eta$ is a zero-mean Gaussian process. The standard deviation of $\eta$ is selected such that the output of $w_b$ has a $3\sigma$ value of about 200 $\mu$rad .

## 2.1 Simulation Results

For this part of the study, an investigation of the relative performance between gyro-aided and gyroless attitude determination was examined. For the on-board gyro case, a standard Kalman filter with a gyro propagated model was used for attitude determination. The simulations were run for six cases: 1) ESA only with no non-repeatable (NR) errors, 2) ESA only with NR errors, 3) ESA and imager/sounder (I/S) with no NR ESA errors and no NR I/S errors, 4) ESA and I/S with no NR ESA errors and with NR I/S errors, 5) ESA and I/S with NR ESA errors and no NR I/S errors, and 6) ESA and I/S with both NR ESA errors and NR I/S errors.

The first two cases involve using the ESA only. A Monte Carlo type analysis shows that 200-250 $\mu$rad is about the $3\sigma$ range for this error. With no NR errors in the ESA, the attitude accuracy is within 60 $\mu$rad . With the NR errors in the ESA, this accuracy is degraded to about 200 $\mu$rad . Also, large errors in the yaw angle estimates are due to filter un-observability. The observability of using an ESA combined with gyro measurements in a Kalman filter can be shown by using the simplifying assumption of a constant coefficient system (see [4] for details). A summary of the results is shown in Table 1.

**Table 1 Attitude Errors for Various Sensor Configurations and Error Sources**

| Case | Error Sources | Roll Errors | Pitch Errors | Yaw Errors |
|---|---|---|---|---|
| 1 | no NR ESA | 60 $\mu$rad | 60 $\mu$rad | $1\times10^5$ $\mu$rad |
| 2 | NR ESA | 200 $\mu$rad | 200 $\mu$rad | $1\times10^5$ $\mu$rad |
| 3 | no NR ESA, no NR I/S | 60 $\mu$rad | 60 $\mu$rad | 200 $\mu$rad |
| 4 | no NR ESA, NR I/S | 100 $\mu$rad | 100 $\mu$rad | 200 $\mu$rad |
| 5 | NR ESA, no NR I/S | 100 $\mu$rad | 100 $\mu$rad | 200 $\mu$rad |
| 6 | NR ESA, NR I/S | 200 $\mu$rad | 200 $\mu$rad | 300 $\mu$rad |

From Table 1, using the imager/sounder as another sensor significantly improves the yaw angle estimate. Also, since the magnitude of the non-repeatable errors is assumed to be approximately the same in the ESA and in the imager/sounder assembly, the attitude errors are also approximately equal when adding these errors to each sensor individually (i.e., case four and five). The sixth case involves using both the ESA and imager/sounder assembly with non-repeatable errors added to each sensor. A purely deterministic attitude found using QUEST yields errors which are approximately the same magnitude as case six. Therefore, the addition of gyros does not seem to significantly improve the attitude accuracy.

## 3. STAR TRACKER

In this section, the simulation results using a star tracker with and without gyros are presented. First, the star tracker model and parameters are shown. Then, a covariance analysis is presented in order to determine the optimal orientation of the star trackers. Next, the availability of actual stars for the GOES orbit is shown. Results are then presented using QUEST[1] to determine the spacecraft attitude. An Enhanced QUEST algorithm is also derived which filters sensor noise. Finally, simulation results are presented using gyros and a Kalman filter.

All results shown in this section include the dynamics and external disturbance on the spacecraft. The GOES Flight Software Dynamics Model implements a GOES Attitude and Orbit Control Electronics (AOCE) firmware emulation FORTRAN code, which uses a six degree-of-freedom dynamics model. The initial model was developed to examine the augmentation of the ESA with gyros, and the current capability was developed to compare with actual GOES performance using the ESA. A star tracker and star tracker/gyro were also added into the simulation. The simulation includes rotating solar array inertia effects with fully coupled inertia tensor dynamics, magnetic torquers with ideal torque response, and gravity gradient and solar pressure disturbances.

The star tracker can sense up to six stars in an $8^\circ \times 8^\circ$ field of view with a sampling interval of 0.1 seconds. The catalog contains stars ranging from +1.0 to +6.0 magnitude. The star tracker measures the tangent of two angles, $\beta_1$ and $\beta_2$, resulting in a body vector given by

$$\underline{B}_s = \frac{1}{\sqrt{1+\tan^2\beta_1+\tan^2\beta_2}}\begin{bmatrix}\tan\beta_1\\ \tan\beta_2\\ 1\end{bmatrix} \tag{15}$$

where the z-axis of the star tracker is along the boresight. The star tracker "measurements" are obtained by using

$$\tan\tilde{\beta}_i = \tan\beta_i + v_{s_i}, \qquad i=1,2 \tag{16}$$

where $v_s$ is a zero-mean Gaussian process with a $3\sigma$ value of 87.2665 $\mu$rad (18 arc – sec).

Each star tracker must be positioned so that sun intrusions can be avoided at all times. For the GOES orbit, and available sun shade for the star tracker, the minimum exclusion area (allowing for a 3° safety margin) is from 55° North to 55° South of the Nadir vector. For the single star tracker case, the 55° orientation produces the following order for

knowledge accuracy: (1) roll angle (i.e., about the spacecraft's x-axis) is known most accurately, then (2) yaw angle (i.e., about the spacecraft's y-axis), and (3) pitch angle (i.e., about the spacecraft's y-axis) being the least accurate. Roll is the most accurate since the star tracker is perpendicular to this spacecraft's x-axis. Pitch accuracy is least accurate since the 55° star tracker position leads to the y-axis being the least "orthogonal" axis with respect to the tracker boresight.

For the two tracker case, a covariance analysis was performed in order to determine the optimal orientation. Assuming that each star tracker measures one star for simplicity, the error covariance matrix is given by[5]

$$P = \frac{\sigma^2}{\left|b_1 \times b_2\right|^2}\left[ b_1 b_1^T + b_2 b_2^T + \frac{1}{2}\left(b_1 \times b_2\right)\left(b_1 \times b_2\right)^T \right] \tag{17}$$

where $\sigma$ is the measurement error standard deviation, and $b_1$ and $b_2$ are measurement vectors of each star. For a North-South configuration, these measurement vectors are given by

$$b_1 = \begin{bmatrix} 0 \\ \sin 55^\circ \\ \cos 55^\circ \end{bmatrix} \equiv \begin{bmatrix} 0 \\ s \\ c \end{bmatrix} \tag{18a}$$

$$b_2 = \begin{bmatrix} 0 \\ -\sin 55^\circ \\ \cos 55^\circ \end{bmatrix} \equiv \begin{bmatrix} 0 \\ -s \\ c \end{bmatrix} \tag{18b}$$

Using Equation (18), the covariance in Equation (17) becomes

$$P = \frac{\sigma^2}{2}\begin{bmatrix} 1 & 0 & 0 \\ 0 & \dfrac{1}{c^2} & 0 \\ 0 & 0 & \dfrac{1}{s^2} \end{bmatrix} \tag{19}$$

The next configuration studied was to place the both star trackers 55° North (or South) from Nadir and rotated by an angle $\vartheta$, The measurement vectors for this case are given by

$$b_1 = \begin{bmatrix} c\,\tilde{s} \\ s \\ c\,\tilde{c} \end{bmatrix}, \qquad b_2 = \begin{bmatrix} -c\,\tilde{s} \\ s \\ c\,\tilde{c} \end{bmatrix} \tag{20}$$

where $\tilde{s} \equiv \sin\vartheta$, and $\tilde{c} \equiv \cos\vartheta$. The covariance matrix in Equation (17) for this case is given

$$P = \frac{\sigma^2}{2\left(c^4\tilde{s}^2\tilde{c}^2 + c^2\tilde{s}^2 s^2\right)}\begin{bmatrix} c^2\tilde{s}^2 & 0 & 0 \\ 0 & s^2 + c^4\tilde{s}^2\tilde{c}^2 & c\,s\,\tilde{c} - c^3\tilde{s}^2\tilde{c}\,s \\ 0 & c\,s\,\tilde{c} - c^3\tilde{s}^2\tilde{c}\,s & c^2\tilde{c}^2 + c^2\tilde{s}^2 s^2 \end{bmatrix} \tag{21}$$

In order to determine the optimal rotation angle, a cost function involving roll and pitch errors (i.e., allowing for relaxed yaw error conditions) is defined, given by the sum of the roll and pitch covariances,

$$J(\vartheta) = \frac{\sigma^2}{2\left(c^4\tilde{s}^2\tilde{c}^2 + c^2\tilde{s}^2 s^2\right)}\left(c^2\tilde{s}^2 + s^2 + c^4\tilde{s}^2\tilde{c}^2\right) \tag{22}$$

Minimizing this cost function with respect to $\vartheta$ leads to the optimal rotation given by $\vartheta = 90^\circ$. Therefore, the covariance matrix in Equation (21) becomes

$$P = \frac{\sigma^2}{2}\begin{bmatrix} \frac{1}{s^2} & 0 & 0 \\ 0 & \frac{1}{c^2} & 0 \\ 0 & 0 & 1 \end{bmatrix} \tag{23}$$

Equation (23) shows that the yaw angle contains the smallest error, even though yaw was relaxed for the optimal separation angle. Therefore, comparing Equation (19) and Equation (23) leads to the conclusion that the optimal location for the two tracker case is given by one tracker 55° North and one tracker 55° South from Nadir.

## 3.1 Simulation Results

Figure 1 shows the actual number of stars within the North pointing tracker field of view. There is always a minimum of 2 stars, except for the interval from 2.15 to 2.283 hours. A star with a magnitude of 6.256 was added in this interval for the QUEST solution. Figure 2 shows the number of stars within the South pointing tracker field of view. Stars can be added to the South tracker catalog in order to insure a minimum of two stars, but this was not done, since the North tracker was used for simulations involving one tracker. Figure 3 shows the combined number of stars for both trackers (without the addition of any stars). This shows that a minimum of 4 stars is available for the two tracker case. Also, the percentages of time in the orbit with the number of stars in the field of view are shown by Tables 2 and 3.

**Table 2 North Pointing Star Catalog**

| Number of Stars | Percentage in FOV |
|---|---|
| 0 | 0.0 |
| 1 | 0.625 |
| 2 | 10.972 |
| 3 | 15.625 |
| 4 | 27.709 |
| 5 | 23.958 |
| 6 | 21.111 |

**Table 3 South Pointing Star Catalog**

| Number of Stars | Percentage in FOV |
|---|---|
| 0 | 0.0 |
| 1 | 1.458 |
| 2 | 8.056 |
| 3 | 20.972 |
| 4 | 28.889 |
| 5 | 23.272 |
| 6 | 17.153 |

In this section simulation results using the QUEST and Enhanced QUEST algorithms without gyros are presented. The QUEST algorithm minimizes the following cost function

$$J(A) = \frac{1}{2}\sum_{k=1}^{n}\frac{1}{\sigma^2}\left|\underline{B}_{s_k} - A\,\underline{I}_{s_k}\right|^2 \tag{24}$$

where $A$ is the attitude matrix, and $n$ is the number of stars available. QUEST is a deterministic approach which utilizes a point-by-point solution. Therefore, previous measurements are not utilized in the attitude solution. This algorithm requires at least two star measurements to determine the attitude, so a star is added (as previously described) to the single star tracker case.

In general, the attitude knowledge is determined more accurately as the number of star measurements at one time increases and/or the separation distance between stars increases. This can be seen by the deterministic error covariance, given by[1]

$$P_{\tilde{q}\tilde{q}_k} = \sigma^2 \sum_{k=1}^{n} \left[ I_{3\times 3} - \underline{B}_{s_k} \underline{B}_{s_k}^T \right]^{-1} \tag{25}$$

Figure 4 shows the attitude errors from QUEST determined attitude using a single (North) star tracker. Note the large errors about 2 hours into the simulation corresponds to the point where the star availability is primarily 2 stars with a small separation. Figure 4 also shows the $3\sigma$ bounds from Equation (25). This shows excellent agreement between theory and simulation. Figure 5 shows the attitude errors and $3\sigma$ bounds for the two star tracker case. This shows the significant improvement in attitude knowledge by using two trackers.

In order to further improve the attitude accuracy, an Enhanced QUEST algorithm (EQA) was developed. This is a simple first-order Kalman filter which combines a propagated model with the QUEST determined attitudes. Since gyros are not used for this case, the angular velocity is assumed to be perfect (i.e., given by Equation (6)). This assumption is a poor one, since external disturbances, and control and sensor errors are present in the actual system. Typical control errors using the ESA are shown in Figure 6. This shows the large errors and coupling in the roll/yaw axis. The EQA is given by

$$\hat{\underline{q}}_{k+1}(-) = \exp\left\{ \frac{1}{2} \Omega(\underline{\omega}) \Delta t \right\} \hat{\underline{q}}_k(+) \tag{26a}$$

$$\hat{\underline{q}}_k(+) = (1-\alpha) \hat{\underline{q}}_k(-) + \alpha \tilde{\underline{q}}_k \tag{26b}$$

where $\Delta t = 0.1$ seconds, $\tilde{\underline{q}}_k$ is the QUEST determined attitude at time $t_k$, and $\alpha$ is a scalar gain. This gain was determined by minimizing the attitude errors from the simulated runs. A value which is too small adds tends to neglect measurements, and emphasizes the inadequacy of the approximation in Equation (6). A value which is too large adds too much measurement noise, and tends to neglect model corrections. A value of $\alpha = 0.05$ was determined to be optimal. The EQA covariance is derived by re-writing Equation (26) as

$$\hat{\underline{q}}_{k+1} = \Phi_4 \, \hat{\underline{q}}_k \otimes \left[ \underline{I} + \alpha \left( \left\{ \Phi_4 \, \hat{\underline{q}}_k \right\}^{-1} \otimes \tilde{\underline{q}}_{k+1} - \underline{I} \right) \right] \tag{27a}$$

$$\Phi_4 \equiv \exp\left\{ \frac{1}{2} \Omega(\underline{\omega}) \Delta t \right\} \tag{27b}$$

where $\otimes$ denotes quaternion multiplication (see [2]). The QUEST determined quaternion is written as

$$\tilde{\underline{q}}_{k+1} \approx \begin{bmatrix} \delta\tilde{\underline{q}}_{k+1} \\ 1 \end{bmatrix} \otimes \underline{q}_{k+1} \tag{28}$$

where $\underline{q}_{k+1}$ is the true quaternion, and $\delta\tilde{\underline{q}}_{k+1}$ is a three component error vector. Substituting Equation (28) into Equation (27a), and post-multiplying both sides of the resulting equation by $\underline{q}_{k+1}^{-1}$ yields

$$\hat{\underline{q}}_{k+1} \otimes \underline{q}_{k+1}^{-1} \approx \begin{bmatrix} \delta\underline{q}_{k+1} \\ 1 \end{bmatrix} = \Phi_4 \, \hat{\underline{q}}_k \otimes \underline{q}_{k+1}^{-1} (1-\alpha) + \alpha \begin{bmatrix} \delta\tilde{\underline{q}}_{k+1} \\ 1 \end{bmatrix} \tag{29}$$

Using a first-order approximation yields the following covariance for the EQA

$$P_{\hat{q}\hat{q}_{k+1}} = (1-\alpha)^2 \Phi_3 \, P_{\hat{q}\hat{q}_k} \, \Phi_3^T + \alpha^2 P_{\tilde{q}\tilde{q}_k} \tag{30}$$

where $\Phi_3$ is the state transition matrix of $[\underline{\omega}\times]$. Since this matrix is constant and nearly the identity matrix, the diagonal elements of Equation (30) approach the following steady-state value

$$p_{\hat{q}\hat{q}_k} \approx \frac{\alpha}{2-\alpha} p_{\tilde{q}\tilde{q}_k} \tag{31}$$

Figure 7 shows the attitude errors and bounds from Equation (31) using one star tracker and the EQA. Comparing Figure 7 with Figure 4 shows a significant improvement using the EQA. Figure 8 shows the attitude errors using two trackers and the EQA. Comparing Figure 8 with Figure 5 again shows a significant improvement using the EQA.

In this section, the results using gyros and a Kalman filter are presented. Two gyro cases are simulated. The first case involves the use of a DRIRU-II. The second case involves the use of a SIRU. The parameters for both gyros are summarized in Table 4.

**Table 4 Gyro Parameters**

| Parameters | DRIRU-II | SIRU |
|---|---|---|
| $\sigma_u$ (white noise) | $2.15\times10^{-4}$ $\mu$rad$/\sec^{3/2}$ | $1.55\times10^{-4}$ $\mu$rad$/\sec^{3/2}$ |
| $\sigma_v$ (random walk) | 0.206 $\mu$rad$/\sec^{1/2}$ | 1.6 $\mu$rad$/\sec^{1/2}$ |

The gyro model is shown by Equations (1) and (2). The relative performance of the attitude estimation can be found by numerically iterating the Kalman filter equations to steady state. Farrenkopf[6] obtained an analytic solution for the case when the three attitude error angles are assumed decoupled. Farrenkopf's results for the preupdate and postupdate attitude error standard deviations, denoted by $\sigma(-)$ and $\sigma(+)$, respectively, can be written as

$$\sigma(-) = \sigma\left(\xi^2 - 1\right)^{\frac{1}{2}} \tag{32a}$$

$$\sigma(+) = \sigma(-)/\xi \tag{32b}$$

where

$$\xi = \frac{1}{2}\left[\gamma + \frac{1}{2}S_u + \left(\gamma S_u + S_v^2 + \frac{1}{3}S_u^2\right)^{\frac{1}{2}}\right], \quad \gamma = \left[4 + S_v^2 + (1/12)S_u^2\right]^{\frac{1}{2}} \tag{33a}$$

$$S_u = \sigma_u \Delta t^{\frac{3}{2}}/\sigma, \quad S_v = \sigma_v \Delta t^{\frac{1}{2}}/\sigma \tag{33b}$$

In the limiting case of very frequent updates, the preupdate and the postupdate attitude error standard deviations both approach the continuous-update limit, given by

$$\sigma_\infty = \Delta t^{\frac{1}{4}} \sigma^{\frac{1}{2}} \left(\sigma_v^2 + 2\sigma_u \sigma_v \Delta t^{\frac{1}{2}}\right)^{\frac{1}{4}} \tag{34}$$

Using the parameters in Table 4 in Equation (34), it was determined that the DRIRU-II steady-state error is approximately 2.8 times better (i.e., more accurate) than the SIRU. This is also shown in the simulations. Figures 9 and 10 show the attitude errors using the SIRU for the one tracker and two tracker cases, respectively. Figures 11 and 12 show the attitude errors using the DRIRU-II for the one tracker and two tracker cases, respectively. Comparing Figure 9 to Figure 11, and Figure 10 to Figure 12, it is seen that the DRIRU-II is approximately 2 to 3 more accurate for the attitude knowledge than using the SIRU. Results for the cases without gyros and cases with gyros are shown in Table 5 and Table 6, respectively.

**Table 5 Attitude Error Results Without Gyros**

| Cases Simulated | Roll Error $(\mu\text{rad})\ 3\sigma$ | Pitch Error $(\mu\text{rad})\ 3\sigma$ | Yaw Error $(\mu\text{rad})\ 3\sigma$ |
|---|---|---|---|
| QUEST (1 Tracker) | 60 | 1250 | 900 |
| QUEST (2 Trackers) | 35 | 70 | 50 |
| EQA (1 Tracker) | 12 | 225 | 175 |
| EQA (2 Trackers) | 6 | 10 | 8 |

**Table 6 Attitude Error Results With Gyros**

| Cases Simulated | Roll Error $(\mu\text{rad})\ 3\sigma$ | Pitch Error $(\mu\text{rad})\ 3\sigma$ | Yaw Error $(\mu\text{rad})\ 3\sigma$ |
|---|---|---|---|
| KF, DRIRU-II (1 Tracker) | 3 | 15 | 10 |
| KF, DRIRU-II (2 Trackers) | 2 | 3 | 2.5 |
| KF, SIRU (1 Tracker) | 7 | 30 | 12 |
| KF, SIRU (2 Trackers) | 5 | 9 | 7 |

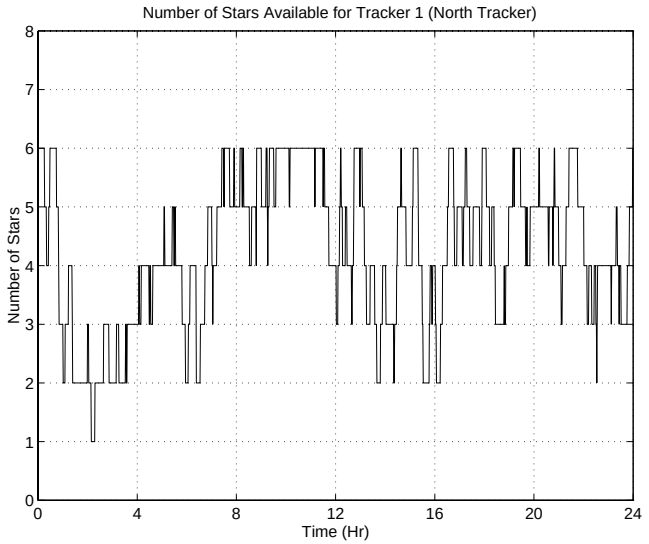


**Figure 1 Availability of Stars for the North Tracker**

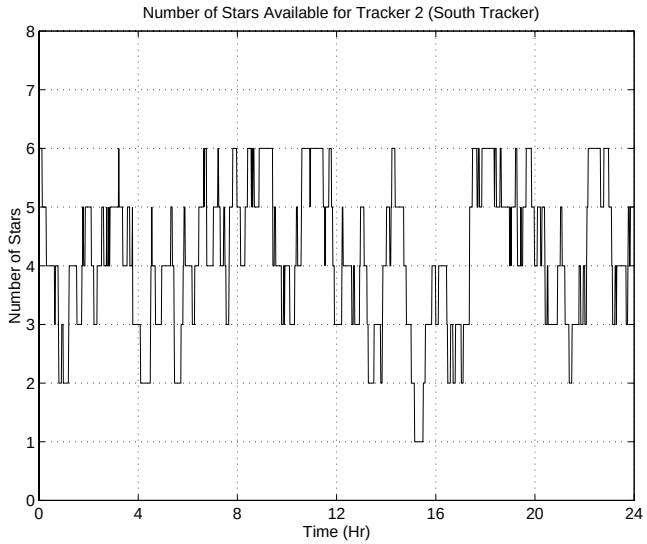


**Figure 2 Availability of Stars for the South Tracker**

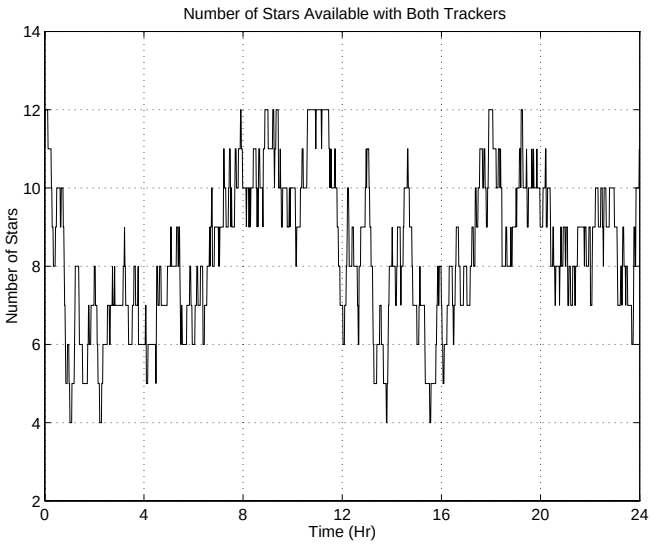


**Figure 3 Availability of Stars for Both Trackers**

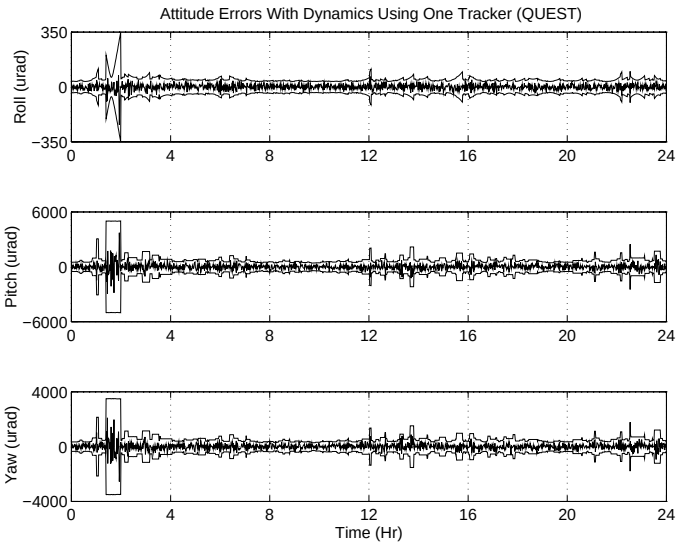


**Figure 4 Attitude Errors and Bounds Using One Tracker (QUEST)**

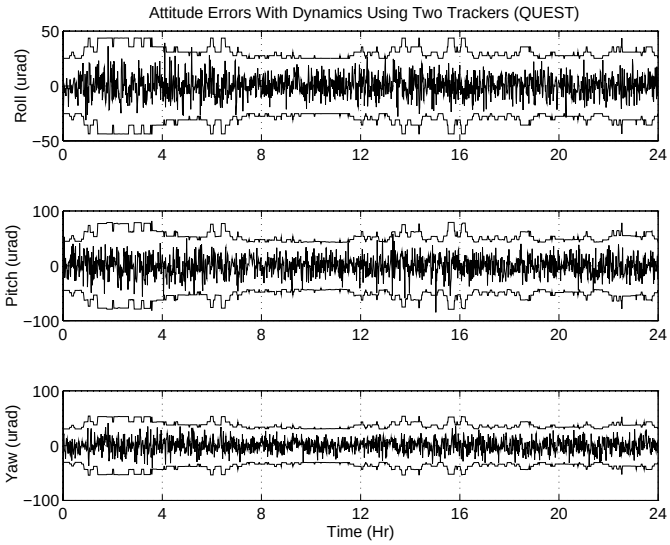


**Figure 5 QUEST Errors and Bounds Using Two Trackers**

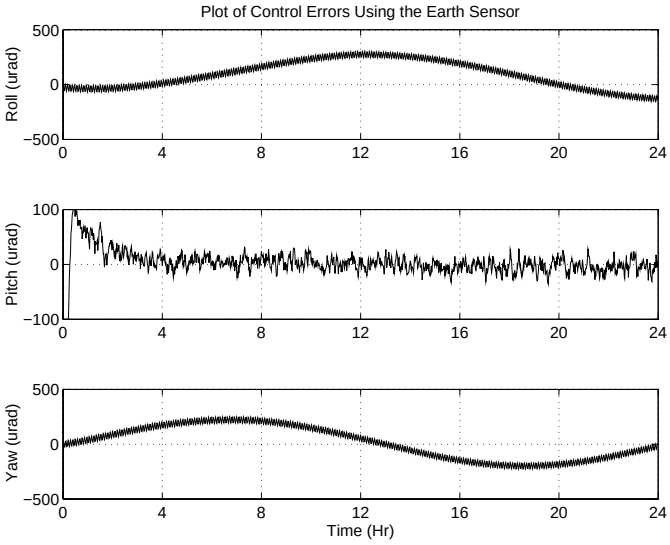


**Figure 6 Control Errors**

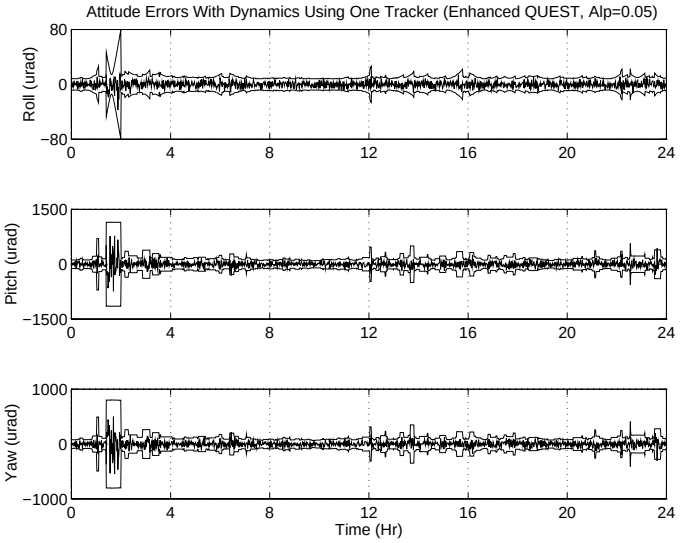


**Figure 7 Attitude Errors and Bounds Using One Tracker (Enhanced QUEST)**

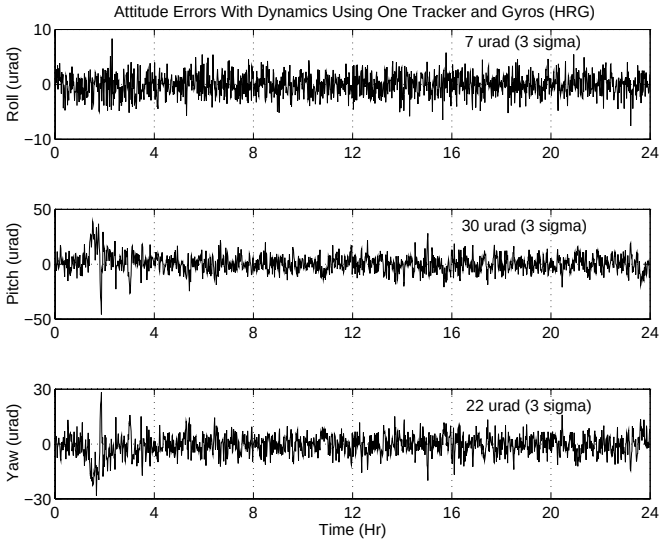


**Figure 9 Attitude Errors Using One Tracker (Kalman Filter, SIRU)**

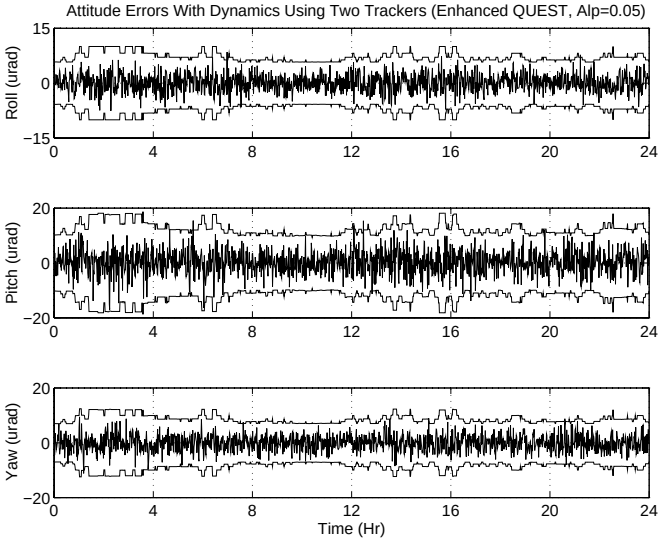


**Figure 8 Attitude Errors Using Two Trackers (Enhanced QUEST)**

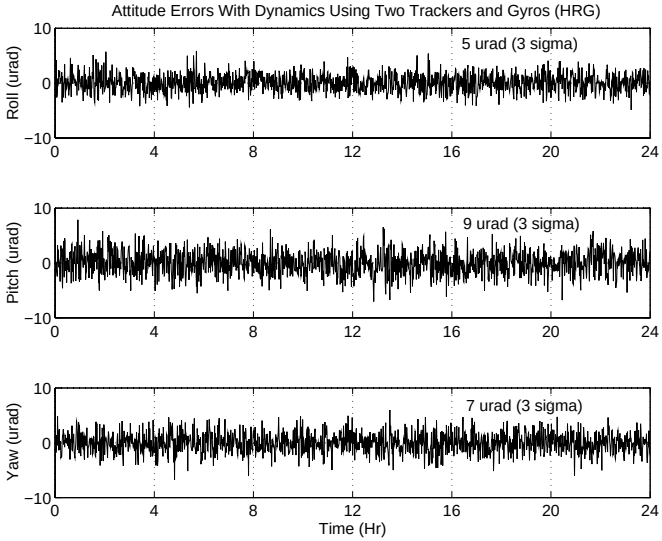


**Figure 10 Attitude Errors Using Two Trackers (Kalman Filter, SIRU)**

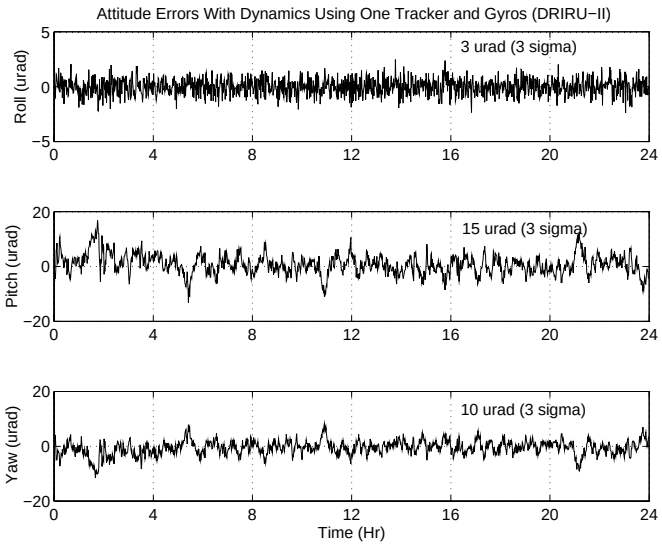


**Figure 11 Attitude Errors Using One Tracker (Kalman Filter, DRIRU-II)**

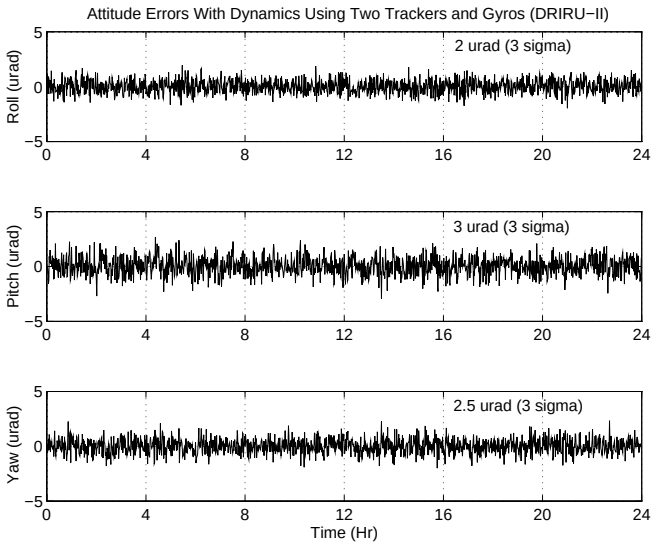


**Figure 12 Attitude Errors Using Two Trackers (Kalman Filter, DRIRU-II)**

## 4. CONCLUSIONS

This study provided some insights for using gyros and/or star trackers on the GOES spacecraft. It was determined that the gyros do not significantly reduce the non-repeatable errors with the ESA. Also, using gyros does not provide any observability in the yaw angle estimate, when using the ESA. The star tracker simulation results show a significant improvement over the ESA attitude knowledge errors. The greatest improvements were shown using either: (1) two trackers with the EQA, or (2) one tracker and a DRIRU-II type gyro, and (3) two trackers and either a SIRU type gyro or a higher quality gyro such as the DRIRU-II. Adding gyros to the spacecraft is the most ideal case, since the Kalman filter bandwidth is larger than the EQA filter bandwidth (i.e., the Kalman filter with gyros can sense higher frequency spacecraft motions than with the EQA). The utilization of on-board gyros may also improve the pointing accuracy, since the controller bandwidth may be increased.

## 5. ACKNOWLEDGMENTS

The first author's work was supported by a National Research Council Postdoctoral Fellowship tenured at NASA-Goddard Space Flight Center. The author greatly appreciates this support.

## 6. REFERENCES

1. M.D. Shuster and S.D. Oh, "Three-Axis Attitude Determination from Vector Observations," *Journal of Guidance and Control*, Vol. 4, No. 1, pp. 70-77, Jan.-Feb. 1981.

2. E.J. Lefferts, F.L. Markley, and M.D. Shuster, "Kalman Filtering for Spacecraft Attitude Estimation," *Journal of Guidance, Control and Dynamics*, Vol. 5, No. 5, pp. 417-429, Sept.-Oct. 1982.

3. Wertz, J.R., (editor) *Spacecraft Attitude Determination and Control*, Kluwer Academic Publishers, Dordrecht, 1978.

4. J.L. Crassidis, F.L. Markley, A.M. Kyle, and K. Kull, "Attitude Determination Improvements for GOES," Proceedings of the Flight/Mechanics/Estimation Symposium, NASA-Goddard Space Flight Center, Greenbelt, MD, pp. 151-165, 1996.

5. F.L. Markley, "Attitude Determination Using Vector Observations: A Fast Optimal Matrix Algorithm," *Journal of the Astronautical Sciences*, Vol. 41, No. 2, pp. 261-280, April-June 1993.

6. R.L. Farrenkopf, "Analytic Steady-State Accuracy Solutions for Two Common Spacecraft Attitude Estimators," *Journal of Guidance and Control*, Vol. 1, pp. 292-284, July-Aug. 1978.